

Investigating mutual coupling in the MWA Phase II compact array

Katherine Elder,¹★ Daniel C. Jacobs,¹

¹*School of Earth and Space Exploration, Arizona State University, Tempe, AZ, USA*

Accepted XXX. Received YYY; in original form ZZZ

ABSTRACT

Measurement of the power spectrum of high redshift 21 cm emission from neutral hydrogen probes the formation of the first luminous objects and the ionization of intergalactic medium by the first stars. However, the 21 cm signal at these redshifts is orders of magnitude fainter than astrophysical foregrounds, making it challenging to measure. Power spectrum techniques may be able to avoid these foregrounds by extracting foreground-free Fourier modes, but this is exacerbated by instrumental systematics that can add spectral structure to the data, leaking foreground power to the foreground-free Fourier modes. It is therefore imperative that any instrumental systematic effects are properly understood and mitigated. One such systematic occurs when neighboring antennas have undesired coupling. A systematic in Phase II data from the MWA was identified which manifests as excess correlation in the visibilities. One possible explanation for such an effect is mutual coupling between antennas. We have built a numerical electromagnetic software simulation of the antenna beam using FEKO to estimate the amplitude of this effect for multiple antennas in the MWA. We also calculate coupling predicted by the re-radiation model which is found to be somewhat lower than the coupling coefficients produced by the simulation. We find that with many approximations both types of mutual coupling predictions are somewhat lower than the minimum necessary to detect the brightest 21 cm models. However more work is necessary to better validate the required level of coupling and to verify that approximations did not underestimate the level of coupling.

Key words: dark ages, reionization, first stars – instrumentation: interferometers – methods: analytical

1 INTRODUCTION

The redshifted 21 cm emission from neutral hydrogen signal is a key probe of the Cosmic Dawn and Epoch of Reionization (EoR), the period of cosmic history when the first stars and galaxies formed and reionized the intergalactic medium. Detecting this signal will provide insight into the evolution of stars and galaxies. There are a number of radio interferometry experiments currently targeting the cosmological 21 cm power spectrum, including the Murchison Widefield Array (MWA; Tingay et al. 2013a; Wayth et al. 2018) and the Hydrogen Epoch of Reionization Array (HERA; DeBoer et al. 2017; Berkhout et al. 2024).

One of the biggest challenges in detecting the 21 cm signal is distinguishing it from the extremely bright astrophysical foregrounds, which are 10 to 10⁸ times brighter than the 21 cm signal (Santos et al. 2005). Because foreground emission is spectrally smooth while 21 cm emission is not, foregrounds can be suppressed to a “wedge” in the 2D power spectrum, which leaves a region where the 21 cm signal is observable. This is known as the “EoR window” (Pober et al. 2013). Systematic effects within the array can cause the foregrounds to contaminate the EoR window and obscure the 21 cm signal. It is estimated that systematics must be reduced to approximately -35 dB below the 21 cm signal in order to avoid this leakage.

Kolopanis et al. (2023) discovered an unidentified systematic while investigating the shortest baselines in the MWA Phase II data. These baselines had previously been ignored because they did not calibrate

well, but short baselines are the most sensitive to the EoR signal so further investigation was warranted. One of the hypothetical causes of this systematic is mutual coupling between tiles. This paper examines this hypothesis.

The MWA, described in more detail below, is an interferometer with phased array tiles of bowtie dipoles as the primary antennas. Given their relatively low profile and reactive baluns, the tiles have here-to-for thought to have relatively low cross-coupling, though this has not ever been shown in the literature.

Mutual coupling between antennas has been investigated in other instruments (Kern et al. 2019, 2020; Rath et al. 2024). Current upper limit papers for 21 cm experiments report excess correlation above the expected noise level and cite mutual coupling as a potential source (Ali et al. 2015; Beardsley et al. 2016; Kern et al. 2019, 2020; Mertens et al. 2020). Models for how mutual coupling manifests in observations are needed to confidently determine the level of mutual coupling expected. These models can then be compared to observations to determine if it is reasonable that mutual coupling is the source of excess correlation.

Electromagnetic propagation within an array of antennas can be difficult to model analytically, making numerical electromagnetic (EM) simulations the gold standard for obtaining an accurate model. However, the computational demands of such simulations for a large array are high and limit the amount of parameter space that can be explored, motivating an approximate method. In previous studies of mutual coupling, Josaitis et al. (2022); Rath et al. (2024) developed an approximation assuming each antenna re-radiates some fraction of received power. The radiation is assumed to propagate freely ac-

★ E-mail: kat.elder@asu.edu

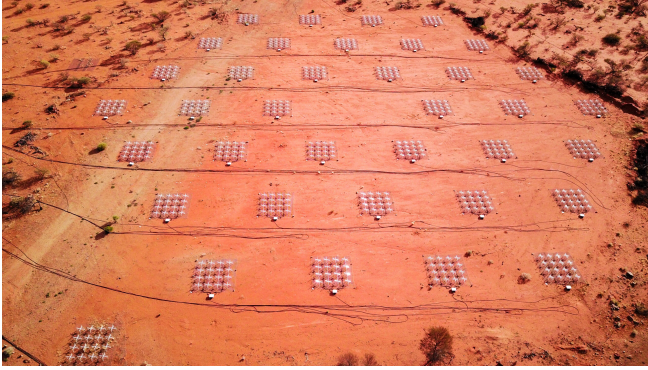


Figure 1. MWA Phase II hexagonal subarray as seen from above. Each tile is made up of a 4x4 grid of individual bowtie dipoles on a 5x5-meter ground plane (Image credit: MWA Project, Curtin University).

cording to the far field approximation. This model ignores reflection off the antenna itself, the effect of intervening antennas along the propagation path, and the effect of multi-path propagation. Multi-path can potentially be incorporated into the analytic model but the others require a more physically accurate simulation. In this paper we aim to understand the coupling between MWA tiles and use the opportunity to compare EM and analytic models. The study is limited to a single MWA Hexagonal subarray.

The approach followed here is to study coupling between MWA tiles using the recent approximate method as well as numerical EM simulation of three MWA tiles, which is the limit of a computationally tractable size. The simulation set also includes a single tile and dual tile setup. We use the S-parameters predicted by the EM simulations to calculate the equivalent coupling for direct comparison to that predicted by the re-radiation model. Armed with a rough validation of the re-radiation model, we calculate the total predicted coupling power on an entire hex subarray and compare to an approximate estimate against the requirement for the coupling to be below predicted 21 cm signals.

2 MURCHISON WIDEFIELD ARRAY

An MWA tile antenna is made up of 16 bowtie dipole elements in a 4x4 grid with 1.1 m spacing between centers. Tiles and dipoles are aligned in the East-West (EW) and North-South (NS) directions. The signals from the 16 dipoles are combined in an analog beamformer which applies a phase delay to the individual antennas to steer the phased array antenna. Each beamformer has both EW and NS linear polarizations. The operating frequency range is 80-300 MHz. See [Tingay et al. \(2013b\)](#) for a more detailed description of the array.

The Phase II upgrade of the MWA ([Wayth et al. 2018](#)) added 256 tile antennas to the array. 72 tiles are arranged in two regular hexagonal configurations near the existing MWA core. The 14 m spacing and hex pattern, which mirrors that used for the HERA telescope, was used because a regular grid allows for higher sensitivity power spectra measurements, as they contain many repeated, or “redundant”, baselines ([Parsons et al. 2012](#)). Figure 1 shows a photo of one of these hex subarrays seen from above. [Wayth et al. \(2018\)](#) reports improved sensitivity on large scales and reduced foreground contamination with the Phase II array power spectrum.

[Kolopanis et al. \(2023\)](#) analyzed data from Phase II of the MWA using the `simpleDS` delay spectrum pipeline. This analysis focused on the three shortest baselines available in the hex subarray, i.e. 14 m,

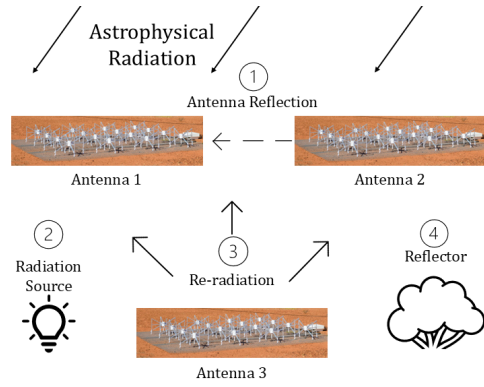


Figure 2. Diagram showing various mechanisms of excess correlation in the visibilities. 1) Signal reflecting off of nearby antennas. 2) A broken cable which allows received sky signal to re-radiate. This causes copies of visibilities to appear in other baselines. 3) Impedance mismatch at the antenna feed causes an antenna to re-radiate the sky signal to the surrounding antennas. 4) An object which is reflecting radiation from the sky back into the array. This can be nearby vegetation, equipment, buildings, etc.

24.24 m, and 28 m. Short baselines have been excluded from previous analysis because their inclusion was found to increase calibration error. However, short baselines are the most sensitive to the Fourier modes expected of the EoR 21 cm signal and they have the most redundant baselines within the hex array.

Inspecting individual baselines, a common mode-type systematic was observed. Excess correlation at delays higher than expected from sky structure was observed to be largely stable across 30 minutes of time but varied widely between nominally redundant baselines. Having established a quality threshold for allowable excess, nearly 50% of all the data from the shortest baselines were found to exceed it. This included 100% of the EW baselines in the data set. Even with these most extreme samples excluded, a power spectrum analysis of the 28 m baselines at redshift 7.14 found a statistically significant detection well above previously established limits. Furthermore, the cross power between different baselines was found to be negative, further suggesting a systematic origin.

[Kolopanis et al. \(2023\)](#) offered two theories on the possible source of this systematic. One possible mechanism is unintended radiation of a broadband signal from somewhere nearby. This would show a dependence on location within the array in both amplitude and phase. Another possible mechanism is the sky signal re-radiated to the surrounding antennas from a broken cable as in [Kern et al. \(2019\)](#). These are both malfunctions in the array operation which might be expected to be fixed with time. A third possibility worth considering because it affects the array as designed is mutual coupling between tiles.

3 MUTUAL COUPLING

Mutual coupling refers to coupling between antennas in radio interferometers, which can cause excess correlation in the visibilities. Figure 2 is a simplified diagram of the various possible sources of excess correlation. These include reflections from nearby antennas or objects; re-radiation from broken connections; and re-radiation from neighboring antennas. We will focus on re-radiation by an antenna. Astrophysical radiation hits all antennas in the array and most of that radiation is absorbed by the antenna. Due to impedance mismatch at the terminals of the antenna feed, some of the radiation is reflected

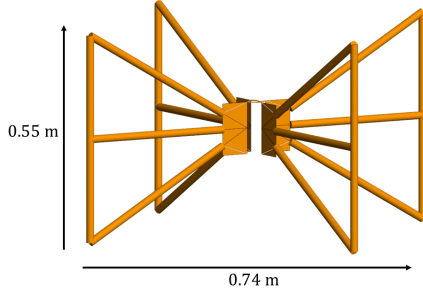


Figure 3. The bow-tie antenna modeled in FEKO.

and re-radiated. This radiation is then absorbed by the surrounding antennas. In this paper, we call this “single path re-radiation”. It is also possible for the re-radiated signal to be reflected off other antennas before being absorbed. We call this “multi-path re-radiation”.

Kern et al. (2019) modeled mutual coupling in HERA as one antenna’s voltage with a coupling coefficient being added to another antenna’s voltage before correlation. This two antenna model was sufficiently descriptive of reality to help develop a filtering technique which reduced amplitude by roughly two orders of magnitude in the power spectrum. While this was an improvement, it was still higher than power spectrum estimates require. Josaitis et al. (2022) derived a more complex model which accounts for a third antenna re-radiating and coupling into a visibility.

In this paper we begin to address the question of mutual coupling in the MWA with a numerical simulation of part of the array described in Section 4. These simulations generate coupling coefficients which can be compared to the re-radiation model which is described in Section 5. Comparing the two in Section 6 we find generally good agreement suggesting the re-radiation model is a reasonably good match. Extending the model to the entire hex in Section 7 we make a crude estimate for the amount of coupling across the entire array and compare that to rough 21 cm requirements on coupling. We close with some discussion about limitations due to approximations and how future work might allow these to be relaxed.

4 NUMERICAL MODEL

A physical model of the bow-tie antenna was built in FEKO¹, a numerical electromagnetic (EM) simulation software. The model is designed to be identical to the original model used by the MWA collaboration (Sokolowski et al. 2017). The FEKO geometry model for a single bowtie dipole was provided by Adrian Sutinjo. It has the same dimensions as the physical dipoles, but uses 15 mm diameter wires rather than aluminum channels to simplify the simulation. The 5x5 m ground plane is modeled as a perfect electrical conductor. Permittivity and conductivity properties of the soil from the Murchison Radio-astronomy Observatory are based on those reported in Sutinjo et al. (2015). We assume the soil is infinite in all directions. Figure 3 shows the bow-tie antenna modeled in FEKO.

The interface between the antenna and the LNA is particularly important in the context of the re-radiation model. In the interest of simplicity, and to match the model used in Sokolowski et al. (2017), the LNA has been modeled as a lumped element circuit. We model the LNA input impedance with a RLC (914 ohm, 450 nH, and 3.2

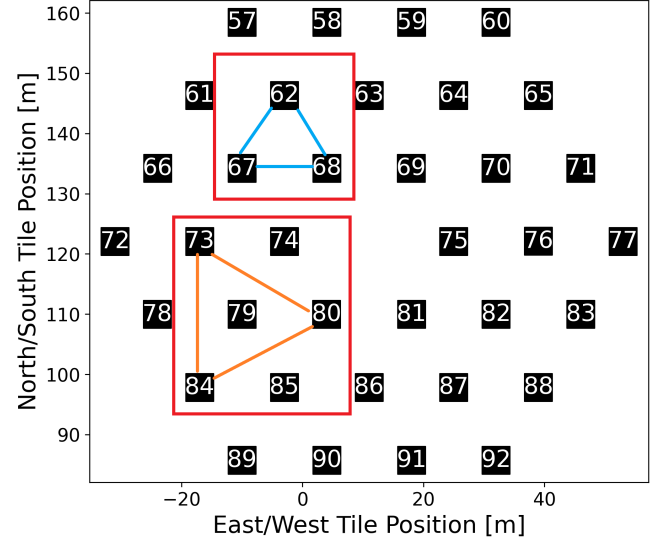


Figure 4. The two redundant baseline vectors used in this analysis plotted over a map of one of the hexagonal arrays. The blue baselines at the top are 14 m, and the orange baselines below are 24.24 m.

pF) shunt network. Sokolowski et al. (2017) reported this as being in agreement with the LNA impedance measured with a vector network analyser.

In Sokolowski et al. (2017), a bowtie dipole is treated as a single embedded element and the far-field radiation pattern $\mathbf{J}(\theta, \phi)$ is measured for each dipole. In this paper, we treat a tile with 16 dipoles as a single embedded element.

To study the effects of mutual coupling on short baselines, we chose the 14 m and 24.24 m to build in FEKO. These are the two shortest and therefore most redundant baselines in the hex subarray. These redundant baselines were built in FEKO, first as two tiles of each baseline length and then as three tiles making up a triangle with the baseline length. Figure 4 shows a map of the hex array with the baselines modeled plotted.

4.1 Simulating re-radiation

The re-radiation model describes a coupling between two antennas. The relevant comparison point against an EM simulation is the S-parameter. S-parameters describe the complex gain factor between two ports in an electrical system. However, the S_{12} simulation will also include factors which have been excluded from the analytic model such as reflection from nearby objects, deviations from far field, resonances between antennas, and non-far-field fringing.

Another advantage of this comparison is that S-parameters are relatively lower cost to calculate. Total FEKO execution time to produce S-parameters for three tiles was 30 hrs compared with 48 hours to calculate far field beams.

First, it is a good idea to check this correspondence in a situation with minimal difference between the broadcast model and an EM solver. A single pair of antennas with a 14 m EW baseline provides no opportunity for multi-path and, at 150 MHz, a 4.4 m tile is reasonably beyond the far field limit at 14 m.²

¹ www.feko.info

² The far field is at $D = 1.22 * \frac{D_{\text{tile}}^2}{\lambda} = 11.8 \text{ m}$

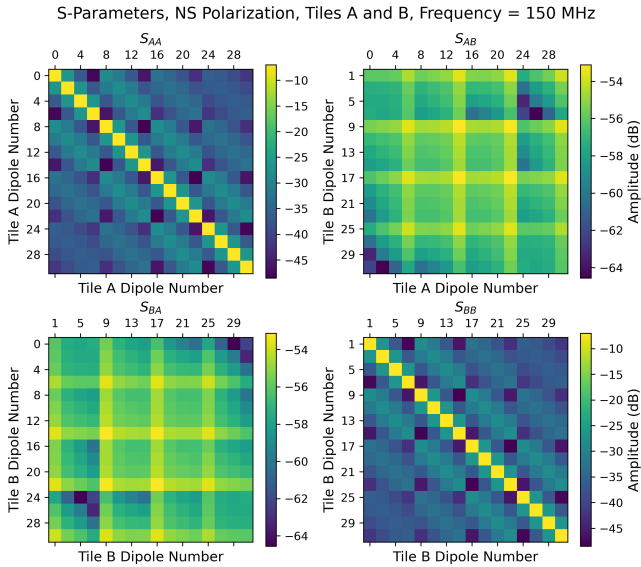


Figure 5. Magnitude of the S-parameter between dipoles in two NS polarized tiles, A and B, with a 14 m EW baseline at 150 MHz. In the S_{AA} and S_{BB} plots, the diagonal corresponds to S_{ii} and block diagonal portions coupling within each tile. The magnitude is lower for larger separation between dipoles. The x- and y-axis labels both correspond to the dipole numbers. The grid pattern of coupling between tiles reflects the distance with closer antennas having higher coupling. We sum over S_{ij} to get the tile level S-parameter.

4.2 Single Baseline S-parameter: re-broadcast check

We use FEKO to calculate the complex S_{ij} between every dipole and sum over each tile for the NS polarization.³ The magnitudes of each S_{ij} were placed into four matrices: one for the S_{ij} between dipoles in Tile A, which will be called S_{AA} ; one for the S_{ij} between dipoles in Tile A and B, which will be called S_{AB} ; one for the S_{ij} between dipoles in Tile B, which will be called S_{BB} ; and one for the S_{ij} between dipoles in Tile B and A, which will be called S_{BA} .

These four matrices are plotted at a single frequency of 150 MHz in Figure 5. The diagonals for the plots of S_{AA} and S_{BB} have higher magnitudes because these correspond to the S_{ii} for each dipole. The magnitude drops off as the distance between dipoles increases, ranging from about -20 to -50 dB. The plots of S_{AB} and S_{BA} are symmetric because the tiles are identical and therefore the measurement is the same regardless of the direction. The grid pattern in the plots of S_{AB} and S_{BA} corresponds to the shape of the tiles and how far apart the dipoles are. The dipoles on the inner edges closest to each other have a magnitude of about -53 to -55 dB, while the dipoles on the outer edges furthest from each other have magnitudes of about -62 to -65 dB. This follows the inverse square law as the distance increases, which fits with the expectation of how mutual coupling behaves over the air.

Each of these matrices is averaged together to produce a single S-parameter value for each tile pair. Figure 6 plots these S-parameters as a function of frequency in MHz. The top plot shows S_{AA} and S_{BB} . These values are equal because of the symmetry of the tiles and therefore appear as a single line plotted on top of each other. There is some spectral structure, with a minimum at ≈ 120 MHz and

S-Parameters, Two Tiles, NS Polarization

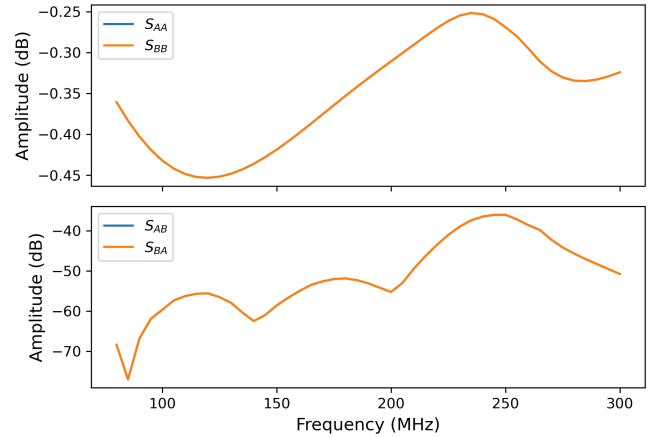


Figure 6. Two plots of the magnitude in dB of the summed S-parameters as a function of frequency in MHz. (top) S_{AA} and S_{BB} are plotted over each other because they are equal. While there is some spectral structure, the range is less than 0.2 dB. (bottom) S_{AB} and S_{BA} are plotted over each other because they are equal. The spectral structure is caused by the shape of the beam in the direction of the other tile.

a maximum at ≈ 245 MHz. However, the range between maximum and minimum is less than 0.2 dB. The bottom plot shows S_{AB} and S_{BA} . These values are equal because of the symmetry of the tiles and therefore appear as a single line plotted on top of each other. The spectral structure of this plot is caused by the shape of the beam in the direction of the other tile. The magnitude goes from around -20 to -70 dB.

4.3 Extending to three antennas

This same analysis was repeated for the three NS polarized tile models and produced similar results for the matrices and the S_{ii} measurements. Figures 7 and 8 show the layout for the two models, with labels indicating the tile names and corresponding S-parameter. Figure 9 shows the comparison of the S_{ij} measurements for the two models. We can see that the 14 m baselines have a higher amplitude, which is to be expected because the tiles are closer together and the EW baseline means the NS antennas are aligned. In both models, the diagonal baselines have lower amplitudes than the horizontal and vertical baselines. A sharp transition occurs at 180 MHz in simulation of the 14 m baseline and only affects the S-parameters involving Tile C. The cause of the transition is unknown. Similar effects were observed in simulations of the EDGES antenna. The root cause was not identified in that case, but were noted in only the Method of Moments solver (Mahesh et al. 2021).

5 RE-RADIATING MODEL

Though EM simulations are potentially the most accurate word on antenna response, there are good reasons to build a simpler model. Numerical simulations are computationally expensive. The three tile FEKO far-field simulation discussed later in this paper took up to 48 hours on a high end desktop. This severely limits exploration of parameter space. Simulations are not necessarily robust. We have found that with reasonable (but ultimately flawed) configurations of the solver, small changes in design can cause large changes in

³ It should be possible to make FEKO model the beamformer as a circuit but we couldn't figure out how to do it.

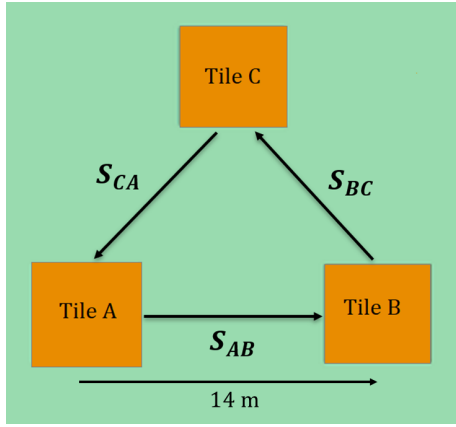


Figure 7. The layout for the three tiles with baseline length of 14 m. This forms an equilateral triangle with an EW baseline. Each tile is labeled with a letter to differentiate them.

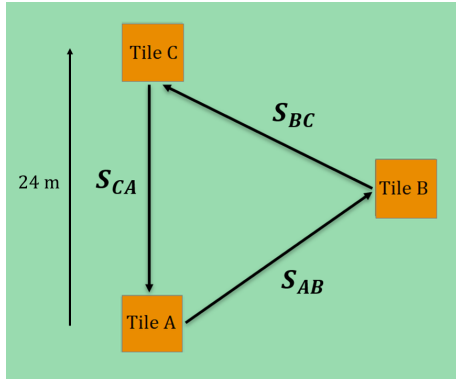


Figure 8. The layout for the three tiles with baseline length of 24 m. This forms an equilateral triangle with a NS baseline. Each tile is labeled with a letter to differentiate them. The tile internal to the triangle is not simulated here.

response. Careful validation by comparison to standard models and between solvers is necessary to build confidence in results. Finally, considering calibration of real data, one might reasonably wish for the results of this study to be a parametrized model which can be solved and inverted to undo effects of mutual coupling in real data. Even if inversion of effects from data is ultimately infeasible, for all of these reasons a simplified physical model will help understand how different effects contribute to the process.

Motivated by all of these factors, Josaitis et al. (2022) proposed a semi-analytic model which assumes an impedance mismatch at the input to the antenna’s amplifier causes some amount of the incident astrophysical radiation to be reflected, which is then re-radiated and absorbed by other antennas in the array. Only single re-radiation paths between antennas are considered; multi-path reflections are ignored. Rath et al. (2024) compared this model to observations from HERA and found that the model does indeed reproduce the observed temporal and spectral behavior of HERA data, however it under-predicts the amplitude by roughly an order of magnitude. This means that while the model can be helpful in devising a time-and-frequency filtering scheme to reduce coupling in the EoR window, the model is an incomplete reflection of reality. The reason for model inaccuracy remains unknown.

The re-radiating model is “semi-analytic” because it relies on numerical EM simulations of isolated antennas to determine quantities

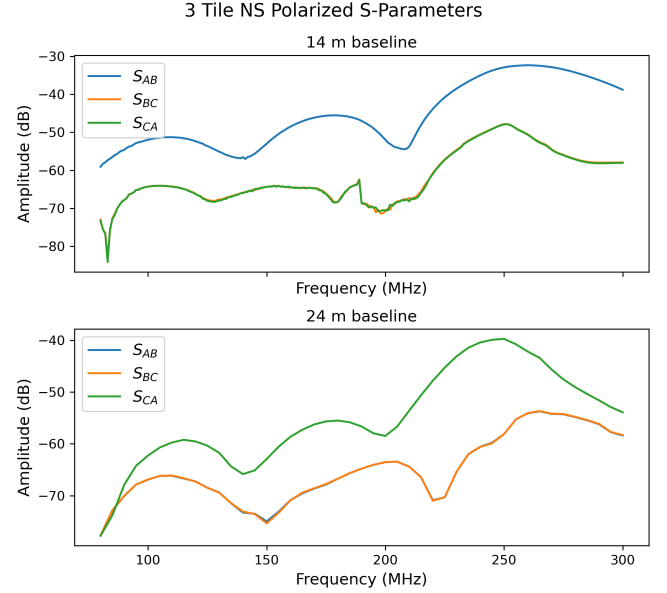


Figure 9. S_{12} simulations of the three tile models, all using NS polarization. For the 14 m configuration (see Fig 8), S_{AB} is the EW baseline and has the highest coupling. The symmetric diagonals S_{BC} and S_{CA} are almost equal. The tiles were positioned using the actual measured locations of the tiles meaning the distances between tiles are not exactly the same. This may account for the slight difference seen. A sharp transition occurs at 180 MHz. The transition only occurs in simulation of the 14 m baseline and only affects the S-parameters involving Tile C. The cause of the transition is unknown. Similar effects were observed in simulations of the EDGES antenna. The root cause was not identified in that case, but were noted in only the Method of Moments solver (Mahesh et al. 2021). In the 24 m baseline simulation (see Fig 8), S_{CA} is the NS baseline and has the highest magnitude of the three. The S_{AB} and S_{BC} measurements are almost equal with slight differences for the same reason as the shorter baseline.

such as the impedance and the radiation pattern for an isolated antenna, and then these results are used to calculate the expected coupling between two antennas. Mathematically the model works out such that each baseline ij has added to it copies of other baselines, specifically those between the two participating antennas and every other antenna in the array. What follows is a short derivation; see Rath et al. (2024) for a more detailed derivation.

The first step is to define the visibilities one expects if no mutual coupling occurs. The electric field from astronomical sources arrives with the single far-field radiation having a Jones matrix:

$$J = \begin{pmatrix} A_{\theta}^p & A_{\phi}^p \\ A_{\theta}^q & A_{\phi}^q \end{pmatrix} \quad (1)$$

where θ, ϕ correspond to the different electric field polarizations and p, q are the feed polarizations.

Writing incoming radiation as Stokes parameters, the linear polarized Coherency matrix is (after Clark in Taylor et al. (1999)):

$$C(\hat{n}) = \begin{pmatrix} I+Q & U+iV \\ U-iV & I-Q \end{pmatrix} \quad (2)$$

where the components of the matrix are written in terms of the Stokes parameters (Josaitis et al. 2022).

The visibility for baseline ij is defined as:

$$V_{ij} = Nh_0^2 \int_{4\pi} J(\hat{n})C(\hat{n})J(\hat{n})^\dagger e^{-i2\pi\nu b_{ij}\cdot\hat{n}/c} d\Omega \quad (3)$$

where N is a normalization constant that converts from V^2 to J_y , h_0 is the effective height⁴, $J(\hat{n})$ is the Jones matrix of the far-field radiation pattern coming from direction \hat{n} normalized to unity at zenith, $C(\hat{n})$ is the coherency matrix, $b_{ij} = x_j - x_i$ is the baseline separating antennas i and j , ν is the frequency at which the visibility is measured, and c is the speed of light in vacuum.

The next step is to add coupling to the “ideal” visibilities. Here the coupling model is limited to a single path coupling between antennas, with a single mechanism for the cause of that coupling. An impedance mismatch between the feed and the rest of the signal chain causes a portion of the incident signal to be reflected and re-radiated from the feed in spherical wavefronts. The re-radiated field E' for a dipole antenna can be written as (Singh et al. 2013):

$$E' = \frac{i\eta_0}{4\lambda} \frac{\Gamma}{R} \frac{e^{i2\pi\nu r/c}}{r} h_0^2 J^\dagger J E \quad (4)$$

where R is the antenna resistance, λ is the wavelength of the radiation, η_0 is the impedance of free space, Γ is the voltage reflection coefficient obtained from the impedance mismatch, and r is the distance from the scattering element.

The “effective height” characterizes the electromagnetic properties of an antenna. Visibility and numerical EM simulators do not calculate effective height, so we need to rewrite h_0 in connection to the far-field radiation pattern. Effective height h is related to the current I in the antenna, and the radiation pattern F is produced by the current via $Ih = F$, and so $Ih_0 = F_0$. Using the power being radiated away by the antenna, we end up with the equality:

$$\frac{\eta_0 h_0^2}{4\lambda^2 R} = \frac{1}{\Omega_p} \quad (5)$$

where Ω_p is the beam area. The coupling coefficient for baseline ik is defined as:

$$X_{ik} = \frac{i\lambda\Gamma}{\Omega_p} \frac{e^{i2\pi\nu b_{ij}/c}}{b_{ik}} J(\hat{b}_{ik})J(\hat{b}_{ki})^\dagger \quad (6)$$

Putting everything together and simplifying, the visibilities with mutual coupling can be expressed as:

$$V_{ij}^{(1)} = V_{ij}^{(0)} + \sum_k \left(V_{ik}^{(0)} X_{jk}^\dagger + X_{ik} V_{kj}^{(0)} \right) \quad (7)$$

where $V_{ij}^{(0)}$ is the original visibility without coupling or “zeroth-order visibility”, and $V_{ij}^{(1)}$ is the visibility adjusted for coupling or “first-order visibility”.

6 COMPARING EM SIMULATION AND RE-RADIATION MODELS

Simulated S-parameters provide an estimate of the total coupling between antennas to the limit of the completeness of the EM model while the re-radiation model makes many approximations and is

⁴ “effective height” is an alternative definition of the gain of an antenna which is found in historical discussions of antenna coupling and so used here.

Re-radiation Model terms for a 14 m baseline, NS Polarized

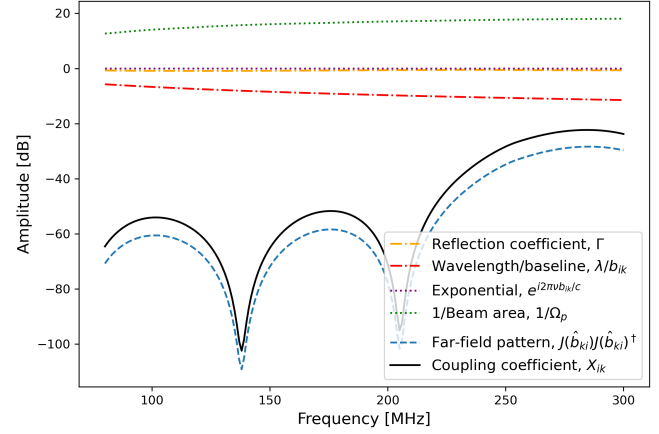


Figure 10. In an illustration of the contributions of the various terms in the re-radiation model. The individual terms of the coupling coefficient are plotted as a function of frequency, calculated here for a NS polarized 14 m EW baseline. The strong spectral dependence is due to nulls in the beam.

known to underestimate the coupling amplitude. Now armed with both varieties of estimate, they can be compared in a few interesting cases.

Eqn. 6 calculates the single path model. FEKO calculates the reflection coefficient, Γ , for each dipole. These individual reflection coefficients are averaged together to determine the reflection coefficient for the entire tile. The beam area, Ω_p , is calculated by squaring the full width at half maximum. $J(\hat{n})$ is the far-field radiation pattern and is dependent on (θ, ϕ) . Here 85° is the lowest available elevation angle due to the beam pattern resolution. Only the NS polarization has been simulated and the EW polarization is determined by a 90 degree rotation. This symmetry is allowed in a single tile simulation used here. The magnitude of the vector field in the direction of the second tile is plugged into Eqn. 6.

Figure 10 shows the amplitude in dB of each term in Eqn. 6 as a function of frequency for the 14 m baseline. X_{ik} is plotted as well to better see how much each term contributes to the final product. We can see that the far-field radiation pattern has the greatest influence on spectral structure. The nulls in the beam move with frequency and only line up with the direction of the neighboring tiles at two frequencies. This can be further confirmed by noting that the spectral period of ≈ 70 MHz corresponds to a physical size ($c/70\text{MHz}$) of ≈ 4 m which is the size of the tile.

Figure 11 shows the comparison of the coupling coefficient, X_{ik} , and S_{ik} for three NS polarized tiles with a 14 m baseline. X_{ik} and S_{ik} have similar spectral structure due to the shape of the beam. X_{ik} has a lower amplitude than S_{ik} and significantly deeper nulls, which is likely due to the reflections present in the multi-path EM model.

7 ESTIMATING IMPACT OF ALL ANTENNAS

Having compared the two coupling models, it is apparent that the re-radiation model is a faithful, if perhaps low, estimate of coupling, particularly in reproducing the expected spectral shape. However, this study so far has been limited to comparisons of a small number of antennas. What is the effect of adding many antennas which would be used in a typical 21 cm power spectrum analysis? In detail this would require a full visibility simulation. Such simulations

Mutual Coupling Models, 3 Tiles, NS Polarized, 14 m Baseline

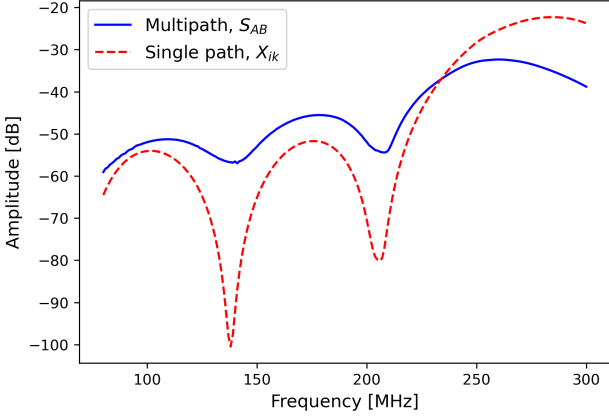


Figure 11. A comparison of numerically simulated S-parameters from FEKO and the calculated coupling coefficient X_{ik} for three NS polarized tiles with 14 m baselines. We observe similar spectral structure, indicating that the shape of the beam is the dominant factor for both quantities. However the coupling coefficient has a lower amplitude by ≈ 5 dB on average and significantly deeper nulls.

require substantial validation and introduce their own uncertainties discussion, which is beyond the scope of this study. However a crude estimate can be made by making the approximation that visibilities on each baseline are roughly the same amplitude. This is true in the case of point sources which dominate longer baselines but not for diffuse structure which dominates the shorter baselines here. In the interest of a first answer, let us ignore diffuse power for now.

Approximating the visibilities to be equal for every baseline, Eqn. 7 becomes:

$$V^{(1)} = V^{(0)} + V^{(0)} \sum_k (X_{jk}^\dagger + X_{ik}) \quad (8)$$

The sum provides a rough approximation of the overall additional power contributed to the visibilities from mutual coupling and can be summed over the full hex subarray.

Figure 12 is a plot of the full hex subarray at a single frequency, with the color scale corresponding to the calculated coupling coefficients for a single tile. Figures 12 and 13 plots the coupling coefficients calculated for an antenna in the middle of the array and at the edge of the array, respectively. The antennas are labeled with the baseline length. Observe how the baseline length is less important than the angle between tiles, as the pattern of peaks and nulls correspond to the shape of the beam. This means that mutual coupling is not uniform across the array and the location of the baseline will affect the level of excess correlation. It also means that redundant baselines will not have identical levels of mutual coupling despite having the same baseline length.

The sum of all of the coupling coefficients is shown in Figure 14 in comparison to the coefficient for a set of three NS polarized tiles with 14 m baselines. The summed coupling coefficient has an interference pattern caused by the number of baselines being added together. Overall, summing across the hex adds 10 dB of coupling amplitude.

The sum for a central tile is just over 1 dB higher than the sum for an edge tile. This is because there are more short baselines in the middle and therefore higher levels of mutual coupling.

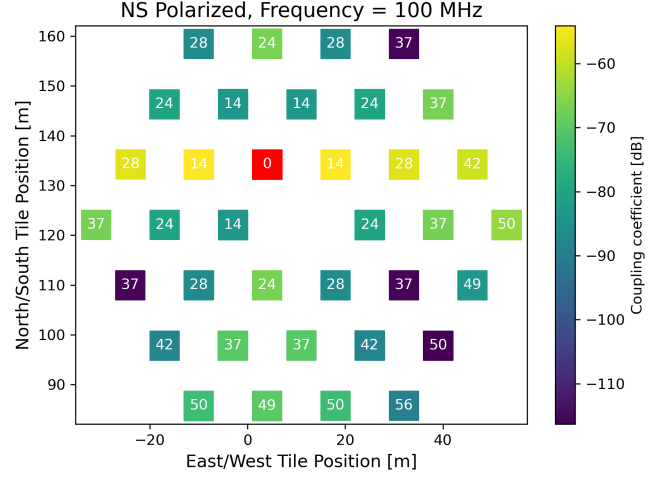


Figure 12. Re-radiation coupling to a NS polarized tile on the edge of the array. The color scale corresponds to the calculated coupling coefficient for that tile at 100 MHz. The label on each tile is the baseline length from the reference tile highlighted in red. It is clear that baseline length is not as important as the direction of another tile. The pattern of the polarization, nulls, and side-lobes clearly maps onto the array.

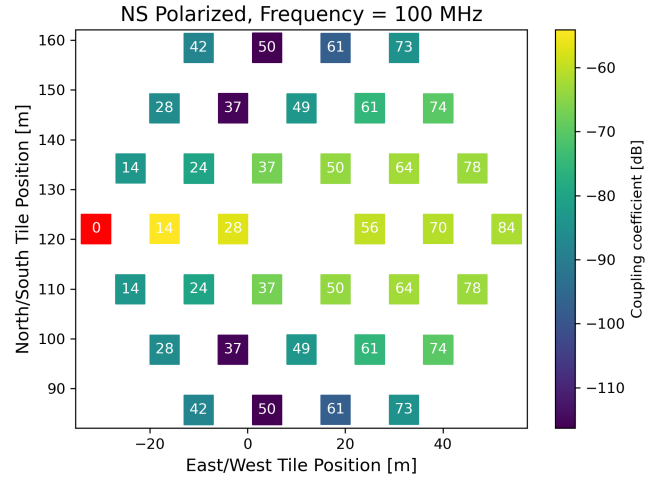


Figure 13. Re-radiation coupling model between red tile and all other tiles in hex. Color scale and polarization same as in Figure 13. The pattern of mutual coupling across the array reflects the beam pattern.

7.1 Coupling requirement for 21-cm work

It is worth considering what is the maximum acceptable level of coupling? Disregarding the spectral axis for now, a rough requirement would hold that the coupling must contribute less than the expected ratio of the foreground power spectrum to the 21 cm signal. Recent limits reported by Trott et al. (2020) report foreground levels at $1e15$ mK^2 and forecasts call for power spectrum levels of 100 mK^2 . This gives a ratio of $1e14$ in power spectrum, $1e7$ in visibility, $1e3.5$ in voltage, or -35 dB.

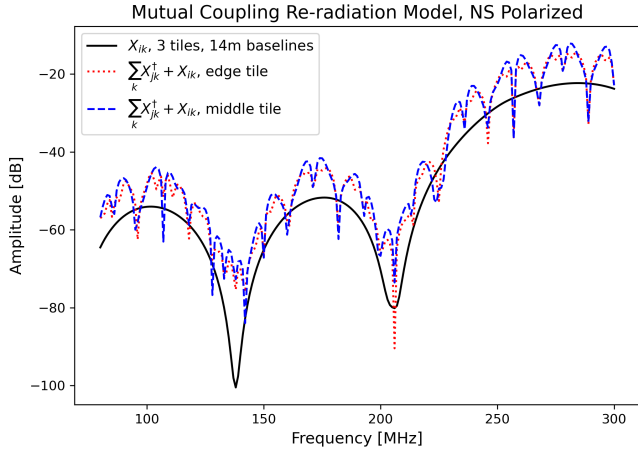


Figure 14. A comparison of the calculated coupling coefficient X_{ik} for three NS polarized tiles with a 14 m baseline and the sum of all baselines. We see that while the overall spectral structure are the same, the summed coupling coefficient is higher by roughly 10 dB.

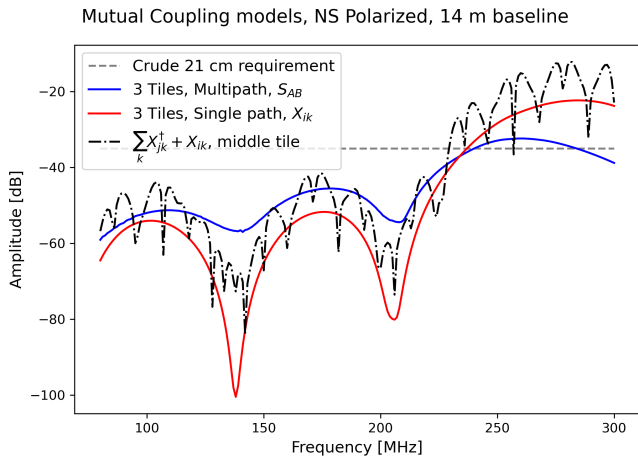


Figure 15. A summary comparison of different mutual coupling models. The numerical S_{ik} simulation of three NS polarized tiles with a 14 m baseline is broadly similar to the re-radiation coupling but higher and with shallower nulls. The sum X_{ik} for three NS polarized tiles with a 14 m baseline is the black dashed line and is the re-radiation coupling across the entire array (assuming all baselines see similar sky). These are all below an estimated maximum allowable isolation -20 dB needed to detect the 21 cm power spectrum, which is plotted as a gray dashed line.

7.2 Summing up

Figure 15 shows the comparison of the amplitude of the multi-path model S_{ik} for three tiles, the single path X_{ik} for three tiles, and the single path $\sum_k (X_{jk}^\dagger + X_{ik})$ for a single central tile, all NS polarized. We can see that S_{ik} is higher than X_{ik} by ≈ 5 dB while the sum of X_{ik} is higher than S_{ik} by ≈ 3 dB. Figure 14 shows that it is only above 240 MHz that the sum of all coupling coefficients reaches -35 dB.

8 CONCLUSION AND DISCUSSION

Mutual coupling between MWA tiles has not been directly studied in the literature. It is not hard to see why. The levels of coupling, at -70 to -40 dB, are relatively low and perhaps difficult to observe in practice.⁵ However the levels are not zero and could pose limitations to power spectrum measurements.

Here we have only considered part of the mutual coupling question, re-radiation. In addition to previous estimates which used a single propagation path and far field approximations, we have calculated numerical simulations of the same paths and found them to be higher amplitude but somewhat smoother in frequency.

8.1 Limitations and Approximations

Several approximations have been made here which limit generalization and motivate future work. The EM simulations used here were kept as small as possible and still show the effect of “multi-antenna” coupling. This allows for only limited multi-path or fringing effects. No surrounding passive environment (such as rocks or trees) was included, nor were any imperfections in the individual tiles. Factors like this have been found to perturb the beam and could introduce further non-redundancy and variation (Chokshi et al. 2024). Future study should include more tiles to explore the impact of multi-path and fringing effects.

In calculating the total effect of all antennas using the re-radiation model, the sky was approximated as roughly the same across all baselines. This neglects the rise in power due to the galaxy on short baselines which will underestimate the amount of contamination these baselines pose to longer baselines. Even restricting to a point source model of the sky, the same assumption also neglects differences between different baseline vectors measuring different phase angles which will tend to cancel power leading to lower observed levels of coupling. On the whole, the summation of all couplings should be regarded as, at best, a crude guide to the true coupling one would observe with the “whole array”.

Finally, the estimated level of maximum allowable coupling for 21 cm experiments is also at best a crude guide and could be improved. A better estimate of the requirement should be done taking into account the “wedge” coupling of foreground power into the 21 cm modes. This would result in a much less strict requirement on coupling, but would apply in specific delay modes where coupling might be relatively stronger. More study is needed in this area.

8.2 Final Thoughts

The original question we sought to answer was how much excess correlation mutual coupling contributes to the MWA and if it was higher than the current EoR power spectrum limits. For three NS polarized tiles with baselines of 14 m, the multi-path S_{ik} model from FEKO is centered around -55 dB at its peaks while the single path re-radiation model is centered around -60 dB at its peaks. If we approximate the visibilities to be identical for all baselines and add all coupling coefficients in the array together, this sum is centered around -45 dB at its peaks. This means that reflections between antennas contributes roughly 5 dB of excess correlation to the visibilities and

⁵ Above 200MHz couplin is significantly higher, reaching as high as -15dB, but the two different models show lower agreement suggesting uncertainty in the models at these higher frequencies. In any case the upper part of the band is not used for 21cm work and has seen limited use due to the strong sidelobes in the tiles.

therefore must be accounted for when addressing mutual coupling. Additionally, increasing from three tiles to 36 tiles increases the level of mutual coupling caused by re-radiation by roughly 8 dB.

We approximate that mutual coupling must be less than -35 dB in order to avoid foreground leakage into the EoR window (Trott et al. 2020). The current models show that it is only above 240 MHz that mutual coupling exceeds that limit, which is above the frequency range for the EoR. However, this is only for the sum of all X_{ik} , which we have already stated underestimates the level of excess correlation. It is therefore likely that if we are able to model all 36 antennas in FEKO to produce a full multi-path approximation, the level of mutual coupling would be higher and exceed this limit at lower frequencies. Further investigation into these two models is needed before specific mitigation suggestions can be made.

ACKNOWLEDGMENTS

This work is supported by the National Science Foundation under grant number AST-2104350.

This scientific work makes use of the Murchison Radio-astronomy Observatory, operated by CSIRO. We acknowledge the Wajarri Yamatji people as the traditional owners of the Observatory site. Support for the operation of the MWA is provided by the Australian Government (NCRIS), under a contract to Curtin University administered by Astronomy Australia Limited. We acknowledge the Pawsey Supercomputing Centre which is supported by the Western Australian and Australian Governments. The MWA Phase II upgrade project was supported by Australian Research Council LIEF grant LE160100031 and the Dunlap Institute for Astronomy and Astrophysics at the University of Toronto.

DATA AVAILABILITY

The inclusion of a Data Availability Statement is a requirement for articles published in MNRAS. Data Availability Statements provide a standardized format for readers to understand the availability of data underlying the research results described in the article. The statement may refer to original data generated in the course of the study or to third-party data analyzed in the article. The statement should describe and provide means of access, where possible, by linking to the data or providing the required accession numbers for the relevant databases or DOIs.

REFERENCES

- Ali Z. S., et al., 2015, *ApJ*, 809, 61
 Beardsley A. P., et al., 2016, *ApJ*, 833, 102
 Berkhout L. M., et al., 2024, *PASP*, 136, 045002
 Chokshi A., Barry N., Line J. L. B., Jordan C. H., Pindor B., Webster R. L., 2024, *MNRAS*, 534, 2475
 DeBoer D. R., et al., 2017, *Publications of the Astronomical Society of the Pacific*, 129, 045001
 Josaitis A. T., Ewall-Wice A., Fagnoni N., de Lera Acedo E., 2022, *Monthly Notices of the Royal Astronomical Society*, 514, 1804
 Kern N. S., Parsons A. R., Dillon J. S., Lanman A. E., Fagnoni N., de Lera Acedo E., 2019, *ApJ*, 884, 105
 Kern N. S., et al., 2020, *ApJ*, 888, 70
 Kolopanis M., Pober J. C., Jacobs D. C., McGraw S., 2023, *Monthly Notices of the Royal Astronomical Society*, 521, 5120
 Mahesh N., Bowman J. D., Mozdzen T. J., Rogers A. E. E., Monsalve R. A., Murray S. G., Lewis D., 2021, *AJ*, 162, 38

- Mertens F. G., et al., 2020, *MNRAS*, 493, 1662
 Parsons A. R., Pober J. C., Aguirre J. E., Carilli C. L., Jacobs D. C., Moore D. F., 2012, *ApJ*, 756, 165
 Pober J. C., et al., 2013, *ApJ*, 768, L36
 Rath E., et al., 2024, *arXiv e-prints*, p. arXiv:2406.08549
 Santos M. G., Cooray A., Knox L., 2005, *ApJ*, 625, 575
 Singh H., Sneha H. L., Jha R. M., 2013, Mutual coupling in phased arrays: A review, doi:10.1155/2013/348123
 Sokolowski M., et al., 2017, *Publications of the Astronomical Society of Australia*, 34, e062
 Sutinjo A. T., et al., 2015, *IEEE Transactions on Antennas and Propagation*, 63, 5433
 Taylor G., Carilli C., Perley R., (U.S.) N. R. A. O., 1999, Synthesis Imaging in Radio Astronomy II: A Collection of Lectures from the Sixth NRAO/NMIMT Synthesis Imaging Summer School Held at Socorro, New Mexico, USA, 17-23 June, 1998. Astronomical Society of the Pacific conference series, Astronomical Society of the Pacific, <https://books.google.com/books?id=e23vAAAAAAAJ>
 Tingay S. J., et al., 2013a, *Publications of the Astronomical Society of Australia*, 30, e007
 Tingay S. J., et al., 2013b, *Publications of the Astronomical Society of Australia*, 30, e007
 Trott C. M., et al., 2020, *MNRAS*, 493, 4711
 Wayth R. B., et al., 2018, *Publications of the Astronomical Society of Australia*, 35, e033

This paper has been typeset from a $\text{\TeX}/\text{\LaTeX}$ file prepared by the author.